Liouvillian Exceptional Points in Quantum Brickwork Circuits

Vladislav Popkov^{1,2} and Mario Salerno³

¹Faculty of Mathematics and Physics, University of Ljubljana, Jadranska 19, SI-1000 Ljubljana, Slovenia ²Department of Physics, University of Wuppertal, Gaussstraβe 20, 42119 Wuppertal, Germany ³Dipartimento di Fisica "E.R. Caianiello", and INFN - Gruppo Collegato di Salerno, Università di Salerno, Via Giovanni Paolo II, 84084 Fisciano (SA), Italy

We demonstrate that Liouvillian exceptional points (LEPs)—previously explored only in continuous Lindbladian dynamics—also emerge in discrete brickwork completely positive trace-preserving (CPTP) circuits. By analytically solving a minimal two-qubit brickwork model, we identify the conditions under which discrete-time LEPs arise and show that they retain the hallmark square-root eigenvalue splitting and linear-in-time sensitivity enhancement. These results establish a direct bridge between continuous non-Hermitian physics and discrete quantum-circuit architectures, opening a path toward the realization of exceptional-point-based sensing on near-term quantum processors.

Introduction.— In the presence of dissipation, the unitary evolution of a quantum system is broken, the map becomes effectively contracting, and the system is driven toward a steady state. Among the possible manifestations of such non-unitary evolution are exceptional points (EPs)—parameter values where the Liouvillian superoperator becomes non-diagonalizable [1, 2]. Liouvillian exceptional points (LEPs) in continuous Lindbladian dynamics promise enhanced sensitivity due to their nonanalytic dependence on perturbations, such as eigenvalue splitting $\propto \sqrt{\varepsilon}$ for a second-order LEP [3–5], analogous to the sensitivity enhancement observed in non-Hermitian photonics [6]. LEPs have recently been demonstrated in continuous-time experiments [7] and analyzed in fewqubit theoretical models [8]. EP-like degeneracies can also appear in auxiliary non-unitary transfer matrices used to compute correlation functions in closed, dualunitary circuits [9]. In that case, however, the EPs pertain to the mathematical construction rather than the physical evolution of the system.

Here we focus on the discrete-time setting most relevant for current quantum devices, where evolution proceeds stroboscopically through brickwork completely positive trace-preserving (CPTP) maps [10–13]. While EPs in non-Hermitian maps and LEPs in continuous Lindbladians have been studied independently, the emergence of LEPs in brickwork CPTP circuits—and the fate of their associated sensing advantages—remain unexplored. The discrete time-step and CPTP constraints could, in principle, alter the Jordan structure or suppress per-step signal amplitudes, challenging the persistence of LEP physics in circuit-based architectures.

In this Letter, we present the first analytic demonstration that two-qubit brickwork CPTP circuits can host Liouvillian exceptional points that retain their characteristic sensing behavior. By constructing minimal steps reproducing a target Lindbladian to first order in Δt , we analytically determine the manifold of LEPs and quantify the eigenvalue-splitting scaling in the discrete-time regime. Our results show that LEPs are a generic fea-

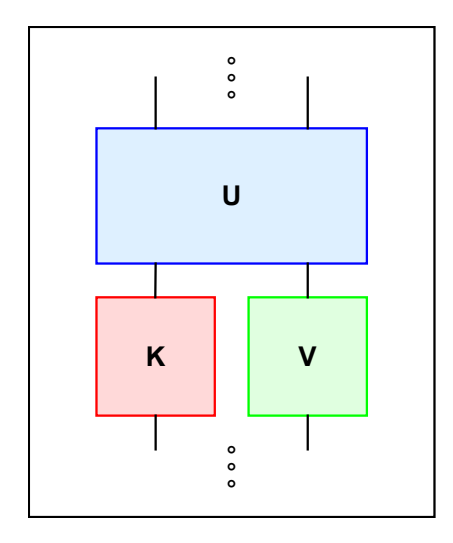


FIG. 1. Schematic of the two-step brickwork protocol. Even steps implement a two-qubit unitary gate U (XXZ-type), while odd steps consist of a Kraus relaxation map on qubit 1 and a local unitary channel V on qubit 2. Periodic repetition of this protocol defines the brickwork CPTP map.

ture of stroboscopic CPTP dynamics, thereby bridging the gap between continuous Lindbladian evolution and the discrete operations implemented in all programmable quantum devices.

Model.— We consider a two-qubit brickwork circuit (Fig. 1), composed of alternating unitary and dissipative layers. Even steps apply a two-qubit gate

$$U = \begin{pmatrix} 1 & 0 & 0 & 0 \\ 0 & a & b & 0 \\ 0 & b & a & 0 \\ 0 & 0 & 0 & 1 \end{pmatrix},\tag{1}$$

parametrized by anisotropy q and spectral parameter λ [14] as

$$a \equiv \frac{q - q^{-1}}{q\lambda - (q\lambda)^{-1}}, \quad b \equiv \frac{\lambda - \lambda^{-1}}{q\lambda - (q\lambda)^{-1}}.$$

In the limit $\lambda \to 1$, U reduces to a Trotterization of the two-qubit XXZ Hamiltonian [10, 11].

Odd steps act locally: qubit 1 undergoes a dissipative Kraus map

$$\mathcal{K}[\rho] = \sum_{j=1}^{2} K_j \rho K_j^{\dagger}, \quad K_1 = \sqrt{1 - \epsilon^2} \, \sigma^+, \quad K_2 = \begin{pmatrix} 1 & 0 \\ 0 & \epsilon \end{pmatrix},$$
(2)

while qubit 2 evolves under an arbitrary local unitary channel $\mathcal{V}[\rho] = V \rho V^{\dagger}$. Here $0 < \epsilon \le 1$ parametrizes the strength of the relaxation of a qubit towards the targeted state $|\uparrow\rangle\langle\uparrow|$ after typical number of steps $n_{\rm relax} = (-2/\log(\epsilon))$ [14].

A full brickwork step is

$$\rho_{t+1} = \mathcal{U}\rho_t = U\left(\sum_{j=1}^2 (K_j \otimes V)\rho_t(K_j^{\dagger} \otimes V^{\dagger})\right)U^{\dagger}, \quad (3)$$

or, in vectorized form, $|\rho[t+1]\rangle = \mathcal{T}|\rho[t]\rangle$, with discrete time Liouvillean (or superoperator)

$$\mathcal{T} = (U \otimes U^*) \left(\sum_{j=1}^2 (K_j \otimes V) \otimes (K_j^* \otimes V^*)^t \right). \tag{4}$$

In the $\Delta t \to 0$ limit, this reduces to a continuous time Lindbladian with jump operator $L = \sigma^+$ acting on the first qubit and XXZ Hamiltonian interactions (see [14]).

Symmetry and block-diagonalization of \mathcal{T} .— Both the Kraus gates and U preserve a \mathbb{Z}_2 parity symmetry, $[\mathcal{K}, \Sigma_z] = [U, \Sigma_z] = 0$ with $\Sigma_z = \sigma_z \otimes \sigma_z$. For the full superoperator to inherit this symmetry we require $[V, \sigma_z] = 0$ in which case V reduces to a pure Z rotation. The superoperator \mathcal{T} can then be block-diagonalized by introducing the parity projectors

$$Q_{\pm} = \frac{1}{2} \left(I_{16} \pm \Sigma_z \otimes \Sigma_z \right), \tag{5}$$

which satisfy $Q_+ + Q_- = I_{16}$, $Q_{\pm}Q_{\mp} = 0$, and $[Q_{\pm}, \mathcal{T}] = 0$. Consequently,

$$\mathcal{T} = Q_+ \mathcal{T} Q_+ + Q_- \mathcal{T} Q_- \equiv \mathcal{T}_+ + \mathcal{T}_-, \tag{6}$$

where \mathcal{T}_{\pm} are rank-8 matrices acting on the even and odd parity subspaces, respectively. Removing null rows and columns yields the effective 8×8 blocks

$$\mathcal{T} = \begin{pmatrix} \tau_+ & 0 \\ 0 & \tau_- \end{pmatrix}. \tag{7}$$

The explicit form of τ_{\pm} are presented in [14].

Superoperator spectrum and EPs manifold. — Although for \mathbb{Z}_2 symmetry the gate V can in general be written as $V = e^{i\theta\sigma_z}$, to gain analytical insight into the spectrum and the location of exceptional points (EPs) we focus, in the following, on the case V = I (i.e. $\theta = 0$),

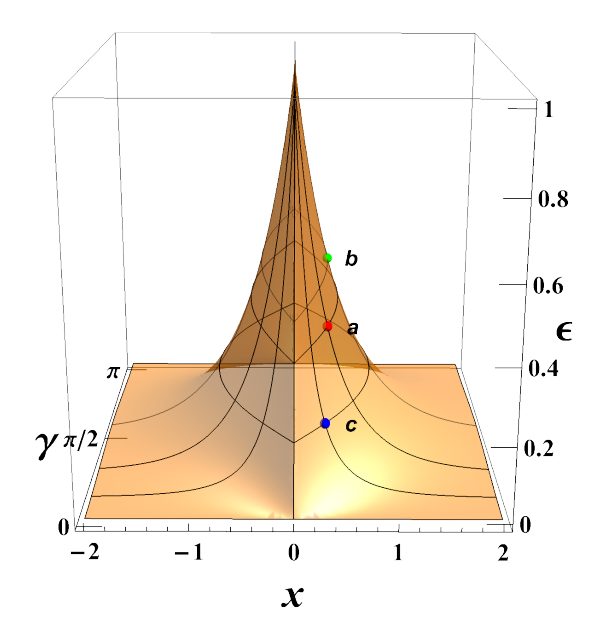


FIG. 2. Superoperator exceptional points manifold in parameter space $\{x \equiv \log \lambda, \gamma, \epsilon\}$ with $\epsilon \in [0,1]$ and $q = e^{i\gamma}$. Coordinates of representative points on the LEP manifold are: $a = \{0.3293, \pi/4, 0.4\}, b = \{0.3466, \pi/2, 0.5\},$ and $c = \{0.3013, \pi/9, 0.2\}$. Bifurcation diagrams of \mathcal{T} eigenvalues for EP a are shown in Fig. 3, while those for EPs b and c are reported in Fig. S-1 of [14].

which we refer to as the *superintegrable* case for reasons given below. This choice preserves the full dependence on (ϵ, q, λ) while considerably simplifying the secular equations of τ_{\pm} , since in this limit the characteristic polynomials factorize into quadratic polynomials [14]. Within this setting, the entire spectrum can be obtained analytically, enabling a complete identification and classification of the non-Hermitian degeneracies that define the EP manifold of the brickwork superoperator.

In particular in the easy-plane regime ($|q| = 1, \lambda \in \mathbb{R}$, $0 < \epsilon \le 1$), the superoperator spectrum acquires a following simple structure: all eigenvalues are either analytic or involve a single square root. Explicitly,

$$\mu_1 = 1, \quad \mu_2 = \epsilon^2, \quad \mu_3 = \mu_4 = \mu_5 = \mu_6 = \epsilon,
\mu_{7,8} = \frac{(Q f \lambda)^2}{4 (q^2 - \lambda^2) (\lambda^2 q^2 - 1)}, \quad \mu_{9,10} = \frac{f \lambda Q}{2(\lambda^2 q^2 - 1)},$$
(8)

$$\mu_{11,12} = \epsilon \mu_{9,10}, \ \mu_{13,14} = \frac{f \lambda Q}{2(q^2 - \lambda^2)}, \ \mu_{15,16} = \epsilon \mu_{13,14},$$

with

$$Q = \sqrt{\lambda^2 (q^4 + 1)(\epsilon - 1)^2 + 2q^2 (2\lambda^4 \epsilon - \lambda^2 (\epsilon + 1)^2 + 2\epsilon)},$$
(9)

$$f = (q^2 - 1)(\epsilon + 1). (10)$$

Denoting $q = e^{i\gamma}$, $\lambda = e^x$, one finds $Q = \sqrt{2}\lambda q\sqrt{A}$

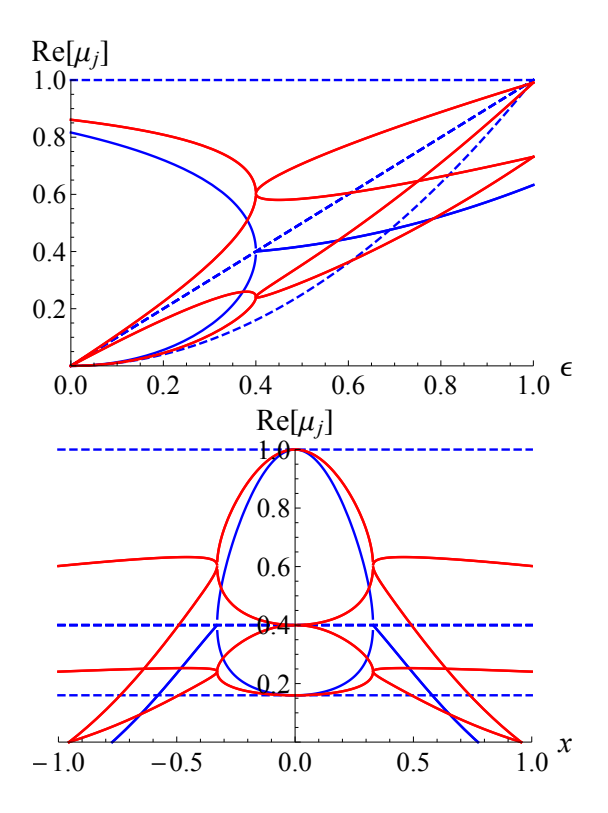


FIG. 3. Real part of \mathcal{T} eigenvalues as a function of ϵ for fixed $\lambda=1.39$ (top panel), and as a function of $\log \lambda$ for fixed $\epsilon=0.4$ (bottom panel). Parameters: $q=e^{i\pi/4},\ V=I$. Red and blue curves correspond to \mathcal{T}_+ and \mathcal{T}_- , respectively, while dashed lines refer to analytic (non-containing EP) eigenvalues $\lambda_j=1,\epsilon,\epsilon^2$. Bifurcation points occur at the EP (red dot), located on the EP manifold shown in Fig. 2.

with

$$A = 2\left((\epsilon - 1)^2\cos(2\gamma) + 4\epsilon\cosh(2x) - (\epsilon + 1)^2\right). \tag{11}$$

The zeros of A correspond to second-order LEPs, i.e., coalescence of two eigenvalues into a Jordan block of size 2×2 . Solving A = 0 yields the EP manifold:

$$\epsilon_{\rm EP} = \frac{\cosh(2x) - \cos^2 \gamma - \sqrt{2}|\sinh x|\sqrt{\cosh(2x) - \cos(2\gamma)}}{\sin^2 \gamma}$$

The function $\epsilon_{\rm EP}(x)$ is even in x and has a cusp at x=0. EP in the 3-dimensional $\epsilon, \lambda, \gamma$ space form a 2D surface, represented in Fig. 2, while Fig. 3 illustrates the eigenvalue bifurcations at the EP.

Sensing properties on the EPs manifold.— To illustrate the impact of EPs on dynamics we consider the discrete-time evolution of observables. For an initial state $\rho[0]$ the vectorized dynamics is

$$|\rho[n]\rangle = \mathcal{T}^n |\rho[0]\rangle, \qquad (13)$$

with \mathcal{T} the superoperator from Eq. (4). Away from EPs, \mathcal{T} is diagonalizable and admits a biorthogonal set of left

 $\{\langle w_j|\}$ and right $\{|v_j\rangle\}$ eigenvectors, $\langle v_j|w_k\rangle=\delta_{jk}$. The expectation value of an observable \hat{g} then reads

$$\langle \hat{g}[n] \rangle = \sum_{j=1}^{16} (\mu_j)^n \, \gamma_j, \quad \gamma_j = \alpha_j \, \text{Tr}(\hat{g} \, \mathbf{v}_j), \quad (14)$$

where μ_j and \mathbf{v}_j are the eigenvalues and eigenmatrices of \mathcal{U} , and $\alpha_j = \langle w_j | \rho[0] \rangle$ are expansion coefficients. Enhanced sensitivity arises when \hat{g} has overlap with eigenvectors associated with an EP.

The cleanest effect of EP can be best seen on observables which have significant overlap with the EP-containing eigenvectors of the superoperator \mathcal{T} , and by choosing an appropriate initial state.

As a concrete example we consider an initially pure quantum state $\rho[0] = |\psi\rangle \langle \psi|$ with $\langle \psi| = 2^{-\frac{1}{2}}(1,0,1,0)$ and take the two-point operator

$$\hat{\mathbf{e}}_3 = \frac{1}{2}\sigma_1^-(I + \sigma_2^z),\tag{15}$$

whose dynamics involves only μ_9, μ_{10} [14]:

$$\langle \hat{\mathbf{e}}_3[n] \rangle = \sum_{j=9,10} (\mu_j)^n \gamma_j \tag{16}$$

with coefficients

$$\gamma_9 = \frac{g_-}{2(4+g_-)}, \quad \gamma_{10} = \frac{g_+}{2(4+g_+)},$$
(17)

and

$$g_{\pm} = \frac{\left(\lambda(q^2 - 1)(\epsilon - 1) \pm Q\right)^2}{(\lambda^2 - 1)^2 q^2 \epsilon}.$$
 (18)

The time evolution of the quantity $|\langle \hat{\mathbf{e}}_3[n] \rangle|$ properly rescaled, is shown on Fig. 4, at EP and its proximity.

Everywhere except at the EP (black curve in the middle row), the numerical data perfectly match the analytic expression (16). An additional factor μ^{-n} in front of the $\langle \hat{\mathbf{e}}_3[n] \rangle$ is chosen so that to ensure that the quantity $|\mu^{-n}|\langle \hat{\mathbf{e}}_3[n] \rangle|$ enters a stable cycle for large n.

Three different regimes can be seen clearly. First, let us discuss the origin of the linear increase at EP (black curve, middle row at Fig. 4). At EP two eigenvalues coincide $\mu_9 = \mu_{10} \equiv \mu_0$ and the respective 2×2 block H of the Liouvillean acquires Jordan form

$$H = \begin{pmatrix} \mu_0 & 1\\ 0 & \mu_0 \end{pmatrix}. \tag{19}$$

A repeated application of the above on a vector $\psi \in C_2$ gives

$$H^n \psi = \begin{pmatrix} \mu_0^n & n\mu_0^{n-1} \\ 0 & \mu_0^n \end{pmatrix} \psi \tag{20}$$

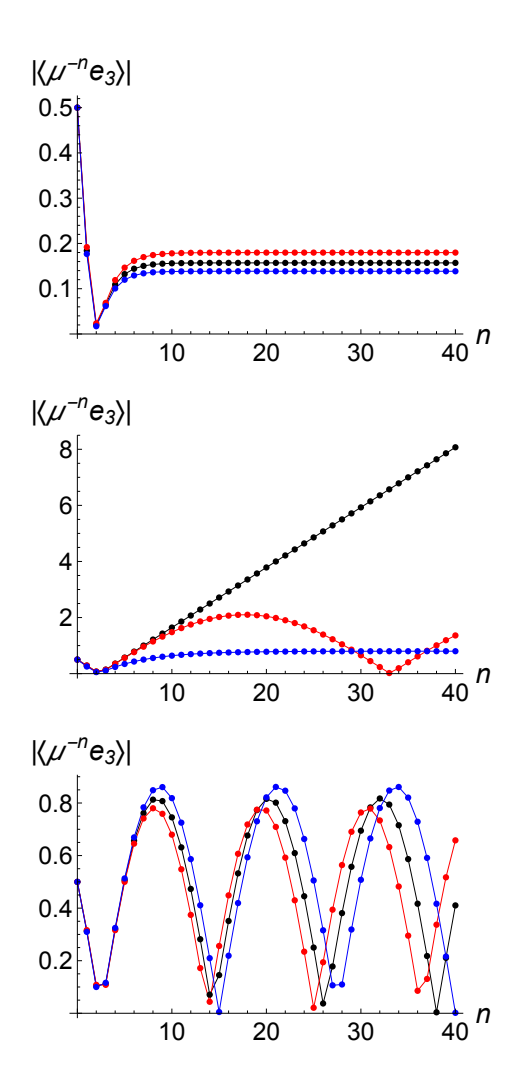


FIG. 4. Renormalized value of $|\langle \hat{\mathbf{e}}_3[n] \rangle|$ versus discrete time n, below EP $\epsilon \equiv \epsilon_0 = 0.32, 0.32 \pm \delta$ (upper row), at EP $\epsilon = 0.4, 0.4 \pm \delta$ (middle row), and above EP $\epsilon = 0.48, 0.48 \pm \delta$ with $\delta = 0.01$. Black, red and blue curves correspond to $\epsilon = \epsilon_0, \ \epsilon_0 + \delta, \ \epsilon_0 - \delta$ respectively. Value of μ is chosen as $\mu = \max(|\mu_9(\epsilon)|, |\mu_{10}(\epsilon)|)$ at the respective ϵ . Linear increase of $|\mu^{-n}\langle \hat{\mathbf{e}}_3[n] \rangle|$ at EP (black curve in the middle row) is due to non-diagonalizability of Liouvillean at EP, see text. Other parameters: $q = \exp(i\pi/4), \lambda = 1.39016$. The EP is located at $\epsilon_{EP} = 0.4$.

Assuming $\psi^T = (a, b)$ we obtain

$$\mu_0^{-n}||H^n\psi|| = \mu_0^{-n} \left\| \begin{pmatrix} \mu_0 & 1\\ 0 & \mu_0 \end{pmatrix}^n \begin{pmatrix} a\\ b \end{pmatrix} \right\|$$
$$= n|\mu_0^{-1}b| \left(1 + O\left(\frac{a}{bn}\right)\right), \tag{21}$$

e.g. an asymptotic linear increase with n, seen on the black curve, in the middle Panel of Fig. 4. Note that if at the point $\epsilon_{EP}=0.4$ the Liouvillean would have conventional degeneracy, i.e. $H=diag(\mu_0,\mu_0)$, then it would result in constant in time $mu_0^{-n}||H^n\psi||=||\psi||=\sqrt{|a|^2+|b|^2}$.

At all the other points except EP we have diagonaliz-

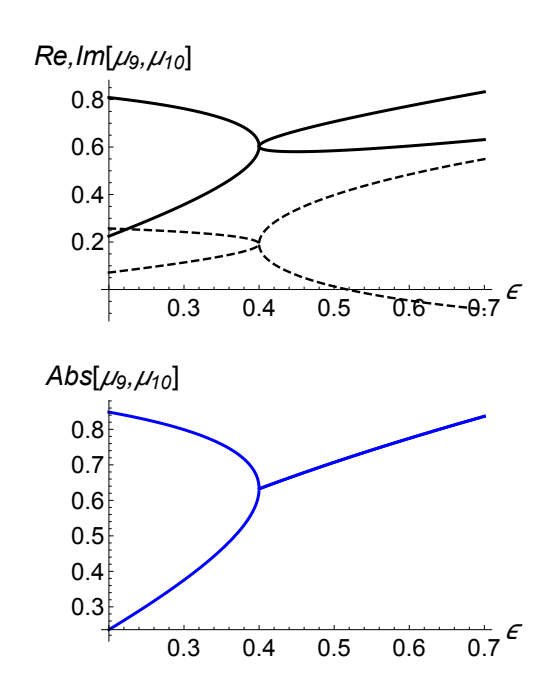


FIG. 5. μ_9, μ_{10} , entering Eq. (16) versus ϵ . EP is located at $\epsilon_{EP} = 0.4$. Bottom Panel shows absolute values $|\mu_9|, |\mu_{10}|$ while the Top panel shows their real part (solid lines) and imaginary part (dashed lines). Other parameters are as in Fig. 4: $q = \exp(i\pi/4), \lambda \approx 1.39$.

able Liouvillean, with temporal evolution of the observable described by (16). However, in particular, there is an asymptotic constant behavior of absolute value of $\mu^{-n}\langle \hat{\mathbf{e}}_3[n] \rangle$ below EP $\epsilon < \epsilon_{EP}$ and an asymptotic periodic behavior above EP $\epsilon > \epsilon_{EP}$. To explain this, let us take a look at the nature of the EP for μ_9, μ_{10} in Fig. 5: above EP, absolute values of μ_9, μ_{10} are the same, while below EP, they are different. This straightforwardly explains the qualitative differences in Fig. 4 for $\epsilon < \epsilon_{EP}$ and $\epsilon > \epsilon_{EP}$.

Conclusion.— We have identified and analytically characterized the full manifold of LEPs in a minimal two-qubit brickwork CPTP circuit. Unlike previous studies of continuous Lindbladians or non- Hermitian Hamiltonians, here LEPs arise naturally in a stroboscopic, noise-inclusive setting relevant to realistic quantum devices. We analytically derived the LEP manifold in the parameter space and showed that near the manifold the dynamics of observables displays the hallmark linear-in-time sensitivity enhancement, demonstrating that discrete-time LEPs preserve the sensing advantages of their continuous counterparts.

In conclusion, our results extend exceptional-point physics, traditionally formulated within continuous Lindbladian dynamics, to discrete architectures built from physical CPTP gates. They identify a universal mechanism for non-Hermitian degeneracies in quantum brickwork circuits and open the possibility of implementing sensing applications on near-term quantum processors.

V.P. acknowledges support by ERC Advanced grant No. 101096208 – QUEST, Research Program P1-0402 and Grant N1-0368 of Slovenian Research and Innovation Agency (ARIS) and by Deutsche Forschungsgemeinschaft through DFG project KL645/20-2. V.P. wishes to thank the Department of Physics of the University of Salerno, where this project initiated, both for hospitality and partial financial support.

See Supplemental Material [14] for: continuoustime limit, explicit forms of τ_{\pm} , derivation of Eq. (8), additional bifurcation diagrams, derivations of Eq. (16-18).

- [1] F. Minganti, A. Miranowicz, R. W. Chhajlany, and F. Nori, Quantum exceptional points of non-hermitian hamiltonians and liouvillians: The effects of quantum jumps, Phys. Rev. A 100, 062131 (2019).
- [2] M. Amato, F. Minganti, and F. Nori, Exceptional points in dissipative quantum systems, Phys. Rev. A 109, 012219 (2024).
- [3] W. Chen, S. K. Ozdemir, G. Zhao, J. Wiersig, and L. Yang, Exceptional points enhance sensing in an optical microcavity, NATURE 548, 192 (2017).
- [4] H. Hodaei, A. U. Hassan, S. Wittek, H. Garcia-Gracia, R. El-Ganainy, D. N. Christodoulides, and M. Khajavikhan, Enhanced sensitivity at higher-order exceptional points, Nature 548, 187 (2017).
- [5] Y.-H. Lai, Y.-K. Lu, M.-G. Suh, Z. Yuan, and K. Vahala, Observation of the exceptional-point-enhanced sagnac effect, NATURE 576, 65 (2019).
- [6] S. Özdemir, S. Rotter, F. Nori, and L. Yang, Parity-time symmetry and exceptional points in photonics, Nat. Mater. 18, 783 (2019).
- [7] W. Chen, M. Abbasi, B. Ha, S. Erdamar, Y. N. Joglekar, and K. W. Murch, Decoherence-induced exceptional points in a dissipative superconducting qubit, Phys. Rev. Lett. 128, 110402 (2022).
- [8] V. Popkov, C. Presilla, and M. Salerno, Manifolds of exceptional points and effective zeno limit of an open two-qubits system, Phys. Rev. A 111, L050202 (2025).
- [9] X.-D. Hu and D.-B. Zhang, Exact correlation functions for dual-unitary quantum circuits with exceptional points, Phys. Rev. B 111, 024301 (2025).
- [10] M. Vanicat, L. Zadnik, and T. Prosen, Integrable trotterization: Local conservation laws and boundary driving, Phys. Rev. Lett. 121, 030606 (2018).
- [11] M. Ljubotina, L. Zadnik, and T. Prosen, Ballistic spin transport in a periodically driven integrable quantum system, Phys. Rev. Lett. 122, 150605 (2019).
- [12] P. Ribeiro and T. Prosen, Integrable quantum dynamics in contact with a bath: Exact results for the kicked liouvillian, Phys. Rev. Lett. 123, 040601 (2019).
- [13] B. Bertini, P. Kos, and T. Prosen, Exact correlation functions in dual-unitary circuit models, Phys. Rev. Lett. 123, 210601 (2019).
- [14] See the Supplemental Material.

Supplemental Material for

"Liouvillian Exceptional Points in Quantum Brickwork Circuits"

Vladislav Popkov¹ and Mario Salerno²

¹ Faculty of Mathematics and Physics, University of Ljubljana, Jadranska 19, SI-1000 Ljubljana, Slovenia ² Dipartimento di Fisica, Università di Salerno, Via Giovanni Paolo II, 84084 Fisciano (SA), Italy

This Supplemental Material provides technical details and extended derivations supporting the results presented in the main text. In Sec. S1, we define the Kraus map and its spectral properties, and clarify its connection to the Lindblad limit. In Sec. S2, we perform the analytical diagonalization of the superoperator \mathcal{T} , derive the explicit expressions for its eigenvalues and identify the emergence of Liouvillian exceptional points (EPs). Additional bifurcation diagrams illustrating the eigenvalue structure are also provided. Section S3 presents the derivation of the time evolution of observables and discusses the role of EPs in their dynamical signatures.

S1. MODEL DETAILS: KRAUS MAP AND CONTINUOUS LIMIT

Model details

Kraus map.— The dissipative channel acting on one of the qubits is defined as

$$\mathcal{K}[\cdot] = \sum_{j=1}^{2} K_j[\cdot] K_j^{\dagger},\tag{S-1}$$

with Kraus operators

$$K_1(\epsilon) = \sqrt{1 - \epsilon^2} \, \sigma_1^+, \qquad K_2(\epsilon) = \begin{pmatrix} 1 & 0 \\ 0 & \epsilon \end{pmatrix}.$$
 (S-2)

This channel is completely positive and trace preserving by construction, as $\sum_j K_j^{\dagger} K_j = \mathbb{I}$. Spectral properties.— The eigenoperators of \mathcal{K} are

$$\psi_0 = |\uparrow\rangle \langle\uparrow|, \qquad \psi_1 = \sigma^z, \qquad \psi_2 = \sigma^+, \qquad \psi_3 = \sigma^-,$$
 (S-3)

with corresponding eigenvalues

$$\lambda_0 = 1, \quad \lambda_1 = \epsilon^2, \quad \lambda_2 = \lambda_3 = \epsilon.$$
 (S-4)

These coincide with those of the channel generated by the Lindblad dissipator $\exp(\Gamma t \mathcal{D}_{\sigma^+})$,

$$\mathcal{D}_L[\rho] = 2L\rho L^{\dagger} - \{L^{\dagger}L, \rho\},\tag{S-5}$$

whose spectrum is

$$\mu_0 = 1, \quad \mu_1 = e^{-2\Gamma t}, \quad \mu_2 = \mu_3 = e^{-\Gamma t}.$$
 (S-6)

The equivalence $\mathcal{K}^n \simeq \exp(\Gamma t \mathcal{D}_{\sigma^+})$ follows in the scaling limit

$$\epsilon = e^{-\Gamma t/n}, \qquad n \to \infty.$$
 (S-7)

Continuous-time limit.— The complete update of the density matrix over one step reads

$$\rho_{t+1} = U\left(\sum_{j=1}^{2} (K_j \otimes V) \rho_t (K_j^{\dagger} \otimes V^{\dagger})\right) U^{\dagger} = \mathcal{U} \rho_t, \tag{S-8}$$

where U is the two-qubit fSim gate defined in Eq. (1) of the main text and V is an arbitrary 2×2 unitary matrix. In the weak coupling limit $\lambda = 1 + \epsilon$ with $\epsilon = (q - q^{-1})t/(in)$ and n very large, we obtain $U \approx I - i\frac{t}{n}h$, where $h = \sigma^x \otimes \sigma^x + \sigma^x \otimes \sigma^x + \frac{q+q^{-1}}{2}(\sigma^z \otimes \sigma^z - I)$ is the density of the XXZ spin chain Hamiltonian. Then, using the Trotter

formula, one obtains $\lim_{n\to\infty} \mathcal{U}^n \rho = e^{\mathcal{L}t} \rho$ where \mathcal{L} is the Liouvillean dynamics of the boundary-driven Lindblad master equation

$$\frac{\partial \rho}{\partial t} = \mathcal{L}[\rho] = -i[H, \rho] + \Gamma \mathcal{D}_{L_{\sigma_1^+}}[\rho], \tag{S-9}$$

where $H = \sum_{n=1}^{N-1} h_{n,n+1}$ is the XXZ spin chain Hamiltonian. Thus, the brickwork circuit can be seen as a generalization of a Trotter discretization of Lindblad dynamics.

Vectorization. — Eq. (S-8) can be recast in the vectorized form

$$|\rho[t+1]\rangle = \mathcal{L}|\rho[t]\rangle,$$
 (S-10)

where \mathcal{L} is the superoperator representation of the combined unitary and dissipative dynamics. From Eq. (S-8), the superoperator reads

$$\mathcal{L} = (U \otimes U^*) \left(\sum_{j=1}^2 (K_j \otimes V) \otimes (K_j^* \otimes V^*)^T \right). \tag{S-11}$$

Unitary regimes.— The fSim gate U is unitary provided either

- (i) |q| = 1 and $\lambda \in \mathbb{R}$ (easy-plane regime), or
- (ii) $q \in \mathbb{R}$ and $|\lambda| = 1$ (easy-axis regime).

In the limit $\lambda \to 1$, U realizes a Trotter step of the XXZ Hamiltonian [10, 11].

S2. ANALYTICAL DERIVATION OF THE SUPEROPERATOR SPECTRUM

 \mathbb{Z}_2 symmetry and block-diagonalization of \mathcal{T} . The invariance under the \mathbb{Z}_2 parity symmetry allows the superoperator \mathcal{T} to be block-diagonalized as follows. Introduce the projectors

$$Q_{\pm} = \frac{1}{2} (I_{16} \pm \Sigma_z \otimes \Sigma_z), \tag{S-12}$$

which satisfy

$$Q_{+} + Q_{-} = I_{16}, \tag{S-13}$$

$$[Q_+, \mathcal{T}] = 0, \tag{S-14}$$

$$Q_{+}Q_{\pm} = 0, \qquad Q_{+}\mathcal{T}Q_{\pm} = 0.$$
 (S-15)

From these relations, \mathcal{T} splits as

$$\mathcal{T} = \mathcal{T}_{+} + \mathcal{T}_{-}, \qquad \mathcal{T}_{\pm} = Q_{\pm} \mathcal{T} Q_{\pm}, \tag{S-16}$$

where \mathcal{T}_{\pm} are rank-8 matrices satisfying $\mathcal{T}_{\pm}\mathcal{T}_{\mp}=0$. Eliminating null rows and columns yields the 8×8 blocks τ_{\pm} :

$$\mathcal{T} = \begin{pmatrix} \tau_+ & 0 \\ 0 & \tau_- \end{pmatrix}. \tag{S-17}$$

The explicit τ_{\pm} matrices can be written in the form

$$\tau_{\pm} = \begin{pmatrix} A_{\pm} & B_{\pm} \\ C \pm & D_{\pm} \end{pmatrix}. \tag{S-18}$$

with respective elements $A_{\pm}, B_{\pm}, C_{\pm}, D_{\pm}$ matrices 4×4 given by:

$$D_{+} = \begin{pmatrix} \frac{\lambda^{2}(q^{2}-1)^{2}}{(q^{2}-\lambda^{2})(\lambda^{2}q^{2}-1)} & \frac{(\lambda^{2}-1)^{2}\epsilon^{2}}{\lambda^{4} - \frac{\lambda^{2}(q^{4}+1)}{q^{2}} + 1} & -\frac{\lambda(\lambda^{2}-1)q(q^{2}-1)\epsilon}{(q^{2}-\lambda^{2})(\lambda^{2}q^{2}-1)} & \frac{\lambda(\lambda^{2}-1)q(q^{2}-1)\epsilon}{(q^{2}-\lambda^{2})(\lambda^{2}q^{2}-1)} \\ \frac{(\lambda^{2}-1)^{2}}{\lambda^{4} - \frac{\lambda^{2}(q^{4}+1)}{q^{2}} + 1} & \frac{\lambda^{2}(q^{2}-1)^{2}\epsilon^{2}}{(q^{2}-\lambda^{2})(\lambda^{2}q^{2}-1)} & \frac{\lambda(\lambda^{2}-1)q(q^{2}-1)\epsilon}{(q^{2}-\lambda^{2})(\lambda^{2}q^{2}-1)} & -\frac{\lambda(\lambda^{2}-1)q(q^{2}-1)\epsilon}{(q^{2}-\lambda^{2})(\lambda^{2}q^{2}-1)} \\ -\frac{\lambda(\lambda^{2}-1)q(q^{2}-1)}{(q^{2}-\lambda^{2})(\lambda^{2}q^{2}-1)} & \frac{\lambda(\lambda^{2}-1)q(q^{2}-1)\epsilon^{2}}{(q^{2}-\lambda^{2})(\lambda^{2}q^{2}-1)} & \frac{\lambda^{2}(q^{2}-1)^{2}\epsilon}{(q^{2}-\lambda^{2})(\lambda^{2}q^{2}-1)} & \frac{\lambda(\lambda^{2}-1)q(q^{2}-1)\epsilon^{2}}{(q^{2}-\lambda^{2})(\lambda^{2}q^{2}-1)} & \frac{\lambda(\lambda^{2}-1)q(q^{2}-1)\epsilon^{2}}{(q^{2}-\lambda^{2})(\lambda^{2}q^{2}-1)} & \frac{\lambda^{2}(q^{2}-1)^{2}\epsilon}{(q^{2}-\lambda^{2})(\lambda^{2}q^{2}-1)} & \frac{\lambda^{2}(q^{2}-1)^{2}\epsilon}{(q^{2}-\lambda^{2})(\lambda^{2}q^{2$$

$$A_{-} = \begin{pmatrix} \frac{\lambda(q^{2}-1)}{\lambda^{2}q^{2}-1} & 0 & \frac{(\lambda^{2}-1)q\epsilon}{\lambda^{2}q^{2}-1} & 0\\ 0 & \frac{\lambda(q^{2}-1)\epsilon^{2}}{\lambda^{2}q^{2}-1} & 0 & \frac{(\lambda^{2}-1)q\epsilon}{\lambda^{2}q^{2}-1}\\ \frac{(\lambda^{2}-1)q}{\lambda^{2}q^{2}-1} & 0 & \frac{\lambda(q^{2}-1)\epsilon}{\lambda^{2}q^{2}-1} & 0\\ 0 & \frac{(\lambda^{2}-1)q\epsilon^{2}}{\lambda^{2}q^{2}-1} & 0 & \frac{\lambda(q^{2}-1)\epsilon}{\lambda^{2}q^{2}-1} \end{pmatrix}, B_{-} = \begin{pmatrix} 0 & 0 & 0 & 0\\ 0 & 0 & -\frac{(\lambda^{2}-1)q(\epsilon^{2}-1)}{\lambda^{2}q^{2}-1} & 0\\ 0 & 0 & 0 & 0\\ 0 & 0 & -\frac{\lambda(q^{2}-1)(\epsilon^{2}-1)}{\lambda^{2}q^{2}-1} & 0 \end{pmatrix}, \tag{S-20}$$

Because of the sparsity of the off-diagonal blocks, the eigenvalues of τ_{\pm} can be computed using the Schur-complement formula:

$$\det(\mu I_8 - \tau_{\pm}) = \det(\mu I_4 - A_{\pm}) \det(\mu I_4 - D_{\pm} - C_{\pm}(\mu I_4 - A_{\pm})^{-1} B_{\pm}) = 0.$$
 (S-21)

Eigenvalues of τ_{+} . From the first factor of Eq. (S-21), four eigenvalues of τ_{+} are directly

$$\mu_{1,2,3,4} = \{1, \epsilon^2, \epsilon, \epsilon\}.$$
 (S-22)

The remaining four eigenvalues follow from the second determinant in the RHS of (S-21) which factorizes as

$$P(\mu) = (\mu - \epsilon)^2 (\mu^2 + \xi \mu + \epsilon^2).$$
 (S-23)

with ξ given by

$$\xi = \frac{\lambda^2 q^4 \left(\epsilon^2 + 1\right) + 2q^2 \left(\lambda^4 \epsilon - \lambda^2 (\epsilon + 1)^2 + \epsilon\right) + \lambda^2 \left(\epsilon^2 + 1\right)}{\left(\lambda^2 - q^2\right) \left(\lambda^2 q^2 - 1\right)}.$$
 (S-24)

Defining

$$f = (q^2 - 1)(\epsilon + 1),$$
 (S-25)

$$Q = \sqrt{\lambda^2 (q^4 + 1)(\epsilon - 1)^2 + 2q^2 (2\lambda^4 \epsilon - \lambda^2 (\epsilon + 1)^2 + 2\epsilon)},$$
 (S-26)

the remaining eigenvalues are $\mu_{5,6} = \epsilon$ and

$$\mu_{7,8} = \frac{(Q \mp f\lambda)^2}{4(q^2 - \lambda^2)(\lambda^2 q^2 - 1)}.$$
 (S-27)

Eigenvalues of τ_{-} . Similarly, the characteristic polynomial of τ_{-} , after clearing common denominators, factorizes into four quadratic monic polynomials:

$$P_1(\mu) = \mu^2 + \frac{f\lambda}{\lambda^2 - q^2} \mu + \epsilon \frac{\lambda^2 q^2 - 1}{q^2 - \lambda^2},$$
 (S-28)

$$P_2(\mu) = \mu^2 + \epsilon \frac{f\lambda}{\lambda^2 - q^2} \mu + \epsilon^3 \frac{\lambda^2 q^2 - 1}{q^2 - \lambda^2},$$
 (S-29)

$$P_3(\mu) = \mu^2 + \frac{f\lambda}{1 - \lambda^2 q^2} \mu + \epsilon \frac{q^2 - \lambda^2}{1 - \lambda^2 q^2},$$
 (S-30)

$$P_4(\mu) = \mu^2 + \epsilon \frac{f\lambda}{1 - \lambda^2 g^2} \,\mu + \epsilon^3 \,\frac{q^2 - \lambda^2}{1 - \lambda^2 g^2},\tag{S-31}$$

with f given in (S-25). It is worth to note that the linear and constant coefficients of the polynomial P_2 are obtained from those of P_1 by multiplication with ϵ and ϵ^2 , respectively, and an analogous relation holds between the pairs P_3 , P_4 . This rescaling of monic quadratic polynomials implies that the roots of P_2 and P_4 coincide with those of P_1 and P_3 , respectively, up to a factor ϵ . Denoting $\mu_{9,\dots,16}$ as the eigenvalues of τ_- , this implies: $\mu_{11,12} = \epsilon \, \mu_{9,10}$, $\mu_{15,16} = \epsilon \, \mu_{13,14}$, with the other eigenvalues following from P_1 and P_3 roots as:

$$\mu_{9,10} = \frac{f\lambda \pm Q}{2(\lambda^2 q^2 - 1)} \qquad \mu_{13,14} = \frac{f\lambda \pm Q}{2(q^2 - \lambda^2)}.$$
(S-32)

This reproduces Eqs. (8) of the main text.

Bifurcation diagrams at points b, c, in Fig. 2 of main text. In Fig. S-1 we depict the bifurcation diagrams of the superoperator matrix eigenvalues as a function of ϵ and of $x = \log(\lambda)$ for parameter values corresponding to points b and c in Fig. 2 of the main text.

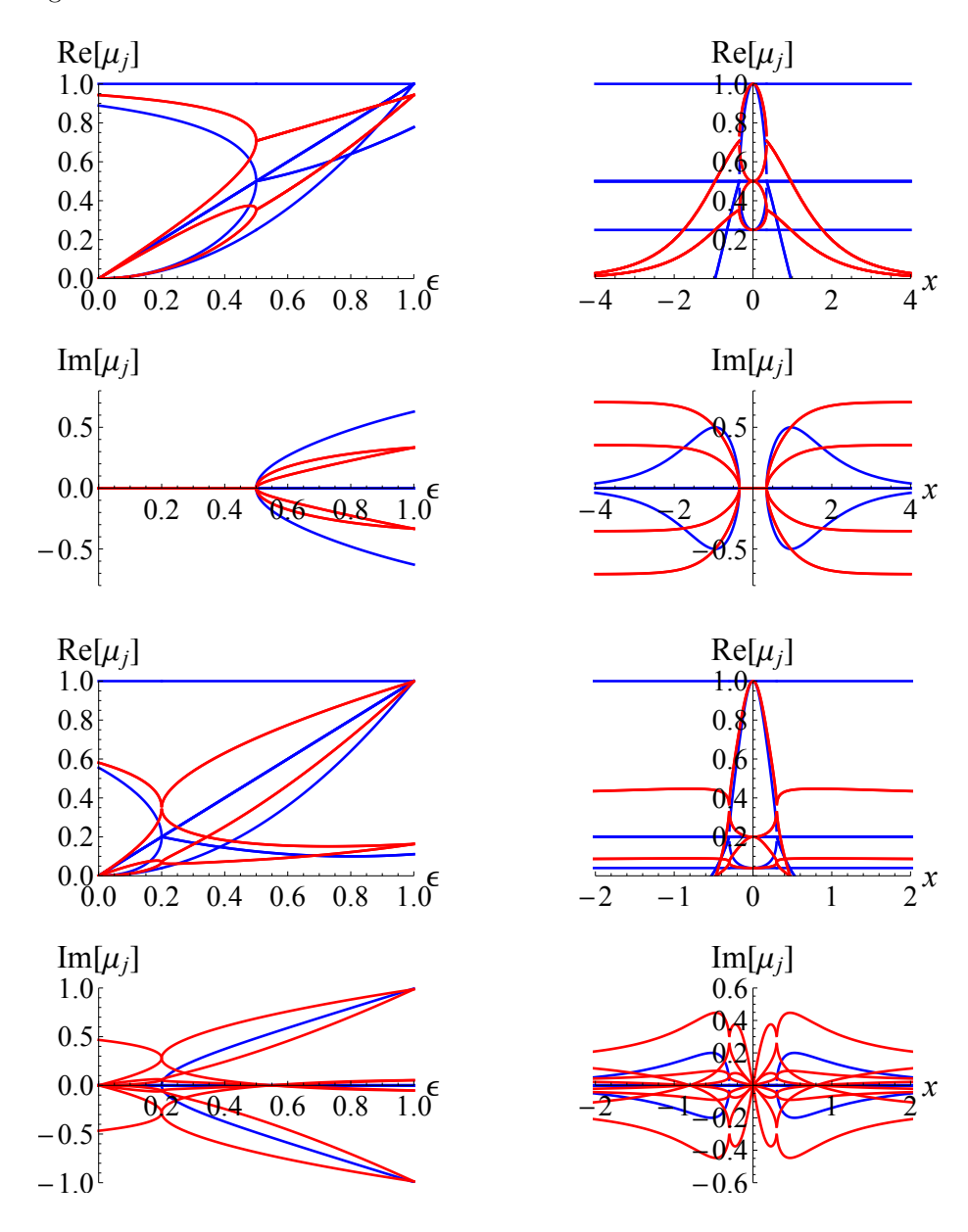


FIG. S-1. Real and imaginary parts of τ_+ (blue color) and τ_- (red color) eigenvalues versus ϵ (left column) and $x = \log(\lambda)$ (right colum), for parameter values corresponding to points b (first and second row panels) and c (third and fourth row panels) in Fig. 2 in the main text.

S3. Time evolution of the observables: derivation of Eqs. (16)-(18).

The diagonalizability of the superoperator \mathcal{T} in Eq. 4 implies the existence of the biorthogonal set of its left and right eigenvectors $\langle w_j|, |u_j\rangle$, corresponding to the eigenvalues μ_j of \mathcal{T} and satisfying $\langle w_j|u_k\rangle = \delta_{j,k}$.

The time evolution of an observable \hat{g} is given by

$$\langle \hat{g}[n] \rangle = \operatorname{tr}(\hat{g}\,\rho[n])$$
 (S-33)

where $\rho[n] = \mathcal{U}^n \rho[0]$ is a reduced density matrix of the system after n steps. Using biorthogonal basis of the vectorized version \mathcal{T} of the map \mathcal{U} we write

$$|\rho[n]\rangle = \sum_{j=1}^{16} (\mu_j)^n \langle w_j | \rho[0] \rangle | v_j \rangle$$
 (S-34)

where $|\rho[n]\rangle$ is a vectorized density matrix after n steps. Using $\langle g|$ for the vectorized version of \hat{g} we obtain

$$\langle \hat{g}[n] \rangle = \sum_{j=1}^{16} (\mu_j)^n \langle w_j | \rho[0] \rangle \langle g | v_j \rangle$$
 (S-35)

In order to see clearly the effect of EP, we need to choose $\rho[0]$ and \hat{g} such that the major contribution in (S-35) comes from some of EP-containing eigenvalues $\mu_7, \mu_8, \dots, \mu_{16}$.

First, we list all the $|v_j\rangle$: using standard notation $(e_j)_k = \delta_{jk}$, we have: for the regular analytic \mathcal{T} eigenvalues $\mu_1, \mu_2, \dots, \mu_6$ the eigenvectors are

$$|v_1\rangle = e_1,$$
 (S-36)

$$|v_2\rangle = e_1 - e_6 - e_{11} + e_{16},$$
 (S-37)

$$|v_{3,4}\rangle = (1+\epsilon)e_1 + x_4e_4 - \epsilon e_6 + Fe_{10} - e_{11} + x_{13}e_{13},$$
 (S-38)

$$|v_{5,6}\rangle = (1+\epsilon)e_1 + x_4e_4 - \epsilon e_6 - Fe_7 - e_{11} + x_{13}e_{13},$$
 (S-39)

$$F = \frac{(1 - q^2)(\epsilon - 1)\lambda}{q(-1 + \lambda^2)},$$
 (S-40)

where x_4, x_{13} are arbitrary constants. The EP-containing eigenvalues contain dependence on the square root Q from (S-26), namely,

$$|v_7\rangle = a_1 e_1 + \sum_{j=6,7,10,11} b_j(Q) e_j,$$
 (S-41)

 a_j are analytic coefficients while $b_j(Q)$ are linear in Q. Then,

$$|v_8\rangle = -|v_7\rangle + 2Q(-\lambda(q^2 - 1))(e_6 - e_{11}) + 2Q(\lambda^2 - 1)q(e_7 - e_{10}).$$
 (S-42)

 $|v_9\rangle, |v_{10}\rangle$ have especially simple form

$$|v_9\rangle = e_5 - \frac{Q - \lambda (q^2 - 1) (\epsilon - 1)}{2 (\lambda^2 - 1) q\epsilon} e_9, \tag{S-43}$$

$$|v_{10}\rangle - |v_9\rangle = -\frac{Q}{(\lambda^2 - 1)q\epsilon}e_9 \tag{S-44}$$

Now, $|v_{11,12,...16}\rangle$ are given by

$$|v_{11}\rangle, |v_{12}\rangle = e_{12} + \sum_{j=2,3,8} d_j(Q)e_j,$$
 (S-45)

$$|v_{13}\rangle = e_2 + \frac{Q - \lambda (q^2 - 1) (\epsilon - 1)}{2 (\lambda^2 - 1) q\epsilon} e_3$$
 (S-46)

$$|v_{14}\rangle - |v_{13}\rangle = \frac{Q}{q\epsilon(1-\lambda^2)} e_3 \tag{S-47}$$

$$|v_{15}\rangle, |v_{16}\rangle = e_{15} + \sum_{j=5,9,14} f_j(Q)e_j$$
 (S-48)

where f_j are some rational expressions containing Q which explicit form will not be needed in the following. Explicit form of the left eigenvectors $\langle w_j |$ can be written as well. With explicit sets $|v_j\rangle$ and $\langle w_j |$ we are in principle able to calculate fully analytically, a time evolution for an arbitrary initial state $\rho[0]$.

Below we shall just give information regarding the chosen observable.

To proceed let us denote by $\hat{\mathbf{e}}_j$ an operator, vectorized version of which is $|\hat{\mathbf{e}}_j\rangle = e_j$. From (S-44), (S-47), we find that among simplest observables \mathbf{e}_j , the two observables

$$\hat{\mathbf{e}}_3 = \frac{1}{2}\sigma_1^-(I + \sigma_2^z), \qquad \hat{\mathbf{e}}_9 = \frac{1}{2}\sigma_1^+(I + \sigma_2^z) = \mathbf{e}_3^{\dagger},$$
 (S-49)

are most sensitive to the presence of EP, since they have an overlap with only EP-containing eigenvectors. Indeed, from easily verifiable $Tr(\mathbf{e}_3\mathbf{e}_j) = \delta_{j,9}$, $Tr(\mathbf{e}_9\mathbf{e}_j) = \delta_{j,3}$, and inspecting (S-36)-(S-48), we find that \mathbf{e}_9 has nontrivial overlap with $|v_{11}\rangle$, $|v_{12}\rangle$, $|v_{13}\rangle$, $|v_{14}\rangle$ only, all of which are EP-containing eigenvectors. Likewise, \mathbf{e}_3 has nontrivial overlap only with $|v_9\rangle$, $|v_{10}\rangle$, $|v_{15}\rangle$, $|v_{16}\rangle$.

Let us choose an observable e_3 for definiteness. From (S-34), we have

$$\langle \hat{e}_3[n] \rangle = \sum_{j=9,10,15,16} (\mu_j)^n \langle w_j | \rho[0] \rangle \langle \hat{e}_3 | v_j \rangle$$
(S-50)

(note that $\langle \hat{e}_3|e_j\rangle=\delta_{j,9}$). To calculate the above, we need explicit form of $\langle w_j|$ for j=9,10,15,16. We find

$$\langle w_{15}| = \frac{q(\lambda^2 - 1)}{Q} \left(e_{14} - f_{-}e_{15} \right),$$
 (S-51)

$$\langle w_{16}| = -\frac{q(\lambda^2 - 1)}{Q} \left(e_{14} - f_{+} e_{15} \right),$$
 (S-52)

$$\left(1 + \frac{f_{-}^2}{\epsilon}\right) \langle w_9 | = e_5 + f_{-} e_9 + A_{14} e_{14} + A_{15} e_{15}, \tag{S-53}$$

$$\left(1 + \frac{f_+^2}{\epsilon}\right) \langle w_{10}| = e_5 + f_+ e_9 + B_{14}e_{14} + B_{15}e_{15}, \tag{S-54}$$

$$f_{\pm} = \frac{\lambda \left(q^2 - 1\right) \left(\epsilon - 1\right) \pm Q}{2 \left(\lambda^2 - 1\right) q},\tag{S-55}$$

where A_{14} , A_{15} , B_{14} , B_{15} are coefficients given by some complicated ratios, explicit form of which will not be needed in the following.

To simplify the calculus further, we choose $\rho[0]$ to be a pure state of the form

$$\rho[0] = |\psi\rangle\langle\psi|, \quad \langle\psi| = \frac{1}{\sqrt{2}}\langle 1, 0, 1, 0|$$
 (S-56)

which has no overlaps with w_{15}, w_{16} : $(w_{15}, |\rho[0]\rangle) = (w_{16}, |\rho[0]\rangle) = 0$. Then the summation in (S-50) extends over j = 9, 10 only. Denoting $\langle w_j | \rho[0] \rangle \langle \hat{e}_3 | v_j \rangle \equiv \gamma_j$, we find

$$\langle \hat{e}_3[n] \rangle = \sum_{j=9,10,15,16} (\mu_j)^n \gamma_j$$
 (S-57)

$$\gamma_{15} = \gamma_{16} = 0,$$
 (S-58)

$$\{\gamma_9, \gamma_{10}\} = \left\{ \frac{g_-}{2(4+g_-)}, \frac{g_+}{2(4+g_+)} \right\}$$
 (S-59)

$$g_{\pm} = \frac{\left(\lambda \left(q^2 - 1\right) (\epsilon - 1) \pm Q\right)^2}{\left(\lambda^2 - 1\right)^2 q^2 \epsilon} = 4\epsilon^{-1} (f_{\pm})^2, \tag{S-60}$$

i.e. Eqs. (16)-(18) of the main text.